Faraday Discussions

RSC Publishing

Cite this: DOI: 10.1039/c3fd00070b

Published on 17 June 2013. Downloaded by National Institutes of Standards & Technology on 04/12/2013 20:37:51.

PAPER

View Article Online
View Journal

Mesoscale inhomogeneities in aqueous solutions of small amphiphilic molecules

Deepa Subramanian,[ab] Christopher T. Boughter,[a] Jeffery B. Klauda,[a] Boualem Hammouda[c] and Mikhail A. Anisimov[ab]

Received 30th April 2013, Accepted 17th June 2013
DOI: 10.1039/c3fd00070b

Small amphiphilic molecules, also known as hydrotropes, are too small to form micelles in aqueous solutions. However, aqueous solutions of nonionic hydrotropes show the presence of a dynamic, loose, non-covalent clustering in the water-rich region. This clustering can be viewed as "micelle-like structural fluctuations". Although these fluctuations are short ranged (~1 nm) and short lived (10 ps–50 ps), they may lead to thermodynamic anomalies. In addition, many experiments on aqueous solutions of hydrotropes show the occasional presence of mesoscale (~100 nm) inhomogeneities. We have combined results obtained from molecular dynamics simulations, small-angle neutron scattering, and dynamic light-scattering experiments carried out on tertiary butyl alcohol (hydrotrope)–water solutions and on tertiary butyl alcohol–water–cyclohexane (hydrophobe) solutions to elucidate the nature and structure of these inhomogeneities. We have shown that stable mesoscale inhomogeneities occur in aqueous solutions of nonionic hydrotropes only when the solution contains a third, more hydrophobic, component. Moreover, these inhomogeneities exist in ternary systems only in the concentration range where structural fluctuations and thermodynamic anomalies are observed in the binary water–hydrotrope solutions. Addition of a hydrophobe seems to stabilize the water–hydrotrope structural fluctuations, and leads to the formation of larger (mesoscopic) droplets. The structure of these mesoscopic droplets is such that they have a hydrophobe-rich core, surrounded by a hydrogen-bonded shell of water and hydrotrope molecules. These droplets can be extremely long-lived, being stable for over a year. We refer to the phenomenon of formation of mesoscopic droplets in aqueous solutions of nonionic hydrotropes containing hydrophobes, as mesoscale solubilization. This phenomenon may represent a ubiquitous feature of nonionic hydrotropes that exhibit clustering in water, and may have important practical applications in areas, such as drug delivery, where the replacement of traditional surfactants may be necessary.

[a]*Department of Chemical and Biomolecular Engineering, University of Maryland, College Park, MD 20742, USA*
[b]*Institute for Physical Science and Technology, University of Maryland, College Park, MD 20742, USA*
[c]*NIST Center for Neutron Research, National Institute of Standards and Technology, Gaithersburg, MD 20899, USA*

Published on 17 June 2013. Downloaded by National Institutes of Standards & Technology on 04/12/2013 20:37:51.

1 Introduction

Properties of aqueous solutions of various small amphiphilic molecules such as C1–C4 monohydric alcohols, amines, and ethers are of great chemical and biological importance. Liquid phases of these solutions are generally considered homogeneous on the macroscopic scale.[1,2] However, recent experimental and computational studies show that they are inhomogeneous over smaller length scales.[3–39] Molecular-scale "clusters" (order of 1 nm in size)[3–21] and, occasionally, mesoscale structures (order of 100 nm in size)[22–39] have been reported in such aqueous solutions.

Simple amphiphiles such as ethanol, *n*-propanol, isopropanol, tertiary butyl alcohol, 3-methylpyridine, 1,4-dioxane, and tetrahydrofuran can be referred to as hydrotropes. Hydrotropes are small amphiphilic molecules that are known to increase the "solubility" of sparingly soluble compounds in water.[40] Hydrotropes are different from traditional surfactants as the hydrotrope molecules have a smaller non-polar tail and do not form distinct micelles in aqueous solutions.[41–43] However, nonionic hydrotropes may show the presence of a dynamic, loose non-covalent "clustering" akin to "micelle-like structural fluctuations".[3–22] Such fluctuations can be detected from molecular dynamics simulations[8,9,12–21] and neutron spin echo experiments.[7] The molecular clusters have a size of the order of 1 nm and a lifetime of tens of picoseconds.[44]

In addition to these molecular-scale inhomogeneities, many experimental works also report the presence of mesoscale inhomogeneities with a size of the order of 100 nm.[23–38] The observed mesoscale inhomogeneities have been a subject of a variety of different explanations: from artifacts and impurities[24] to structural "phase transitions",[23] from microphase separation[36] to clathrate-hydrate precursors,[26] from loose supramolecular clusters[32–34] to kinetically arrested gaseous nanobubbles.[35] The lifetime of these inhomogeneities varies greatly, from hours to years. In our recent works, we have shown that long-lived (practically permanent) mesoscale inhomogeneities in aqueous solutions of hydrotropes originate only when the solution contains at least a trace amount of a third, more hydrophobic, component.[37–39]

In this work, we focus on the mesoscopic properties of one specific nonionic hydrotrope, namely aqueous solutions of tertiary butyl alcohol (TBA). TBA is a "perfect" amphiphile. It is the highest-molecular-weight alcohol isomer to be completely soluble in water at ambient conditions.[1,45] When placed at a water–oil interface, a TBA molecule aligns itself equally between the two phases, such that the hydroxyl group of the TBA molecule is in the water phase and the methyl groups are in the oil phase.[46] The story of aqueous solutions of TBA is full of controversies. The earliest light-scattering experiments in aqueous solutions of TBA were carried out by Vuks and Shurupova in 1972.[23] They observed strong scattering in a solution containing about 3 mol% (11 mass%) TBA. The authors attributed this effect to a possible "phase transition" between a clathrate-like structure and a less ordered structure in the macroscopically homogeneous liquid phase. Beer and Jolly repeated these experiments in 1974 and found that the effect depended on the source and prehistory of the sample.[24] Thus, they regarded the observed strong scattering as an "artifact". In 1977, Iwasaki and Fujiyama carried out light-scattering experiments in a range of aqueous TBA solutions and

 This journal is © The Royal Society of Chemistry 2013

Published on 17 June 2013. Downloaded by National Institutes of Standards & Technology on 04/12/2013 20:37:51.

observed strong scattering in a solution close to 10 mol% (31 mass%) TBA.[25,26] They attributed this effect to the possible existence of clathrate hydrate structures in solution. The idea of clathrate hydrate structures in aqueous TBA solutions was also supported by the X-ray diffraction studies of Tanaka *et al.* and Nishikawa and Ijima.[47,48] The earliest dynamic light-scattering experiments in aqueous TBA solutions were carried out by Euliss and Sorensen in 1984.[27] While studying short-ranged concentration fluctuations in aqueous TBA solutions, they observed the presence of larger (mesoscale) inhomogeneities, of the order of 100 nm in size, in a solution of about 7 mol% (24 mass%) TBA. The authors speculated that this effect might be associated with the formation of clathrates, stabilized by trace amounts of another component. In 1986, Bender and Pecora repeated the experiments of Euliss and Sorensen, and did not observe any mesoscale inhomogeneities.[28] However, when studying aqueous 2-butoxyethanol solutions, Bender and Pecora did observe the presence of mesoscale inhomogeneities ($\sim$100 nm in size).[29] They concluded that the mesoscopic aggregates could be a result of contaminants in the solution.

Debates on the existence of mesoscale inhomogeneities are not unique to aqueous solutions of TBA or 2-butoxyethanol. In 2000, Georgalis *et al.* reported observation of a mesoscale structure (50–500 nm in size) in aqueous electrolyte solutions, namely sodium chloride, ammonium sulfate, and sodium citrate.[30] They attributed the formation of such a structure to hydrogen-bond interactions between water molecules, which act as a bridge for interactions between like-charged ions. In 2004, Yang *et al.* observed mesoscale inhomogeneities (200–600 nm in size) in aqueous solutions of nonionic hydrotropes such as tetrahydrofuran and 1,4-dioxane.[31] They also observed that these inhomogeneities could be removed by filtration, and thus concluded that the effect could be a result of incomplete mixing of water and the organic solute at the molecular scale. In 2006, Sedlák carried out an extensive static and dynamic light-scattering study of around 100 different solute–solvent pairs and observed the presence of large supramolecular aggregates in aqueous solutions of many ionic and non-ionic species.[32–34] Sedlák explained this phenomenon as the formation of a supramolecular structure due to hydrogen-bond interactions between solute and solvent molecules. Soon thereafter, Jin *et al.* in 2007, carried out a static and dynamic light-scattering study in aqueous solutions of various nonionic hydrotropes such as tetrahydrofuran, ethanol, urea, and α-cyclodextrin.[35] The authors observed mesoscopic aggregates of around 100 nm in these systems. They attributed this to the formation of gaseous nanobubbles, which are kinetically stabilized in solution by the adsorption of small amphiphilic molecules on the surface of the nanobubble. Long-lived, mesoscale inhomogeneities were also observed in aqueous solutions of 3-methylpyridine.[36] It was found that these inhomogeneities depended on the source of the sample and thus might be the result of impurities in the solution. In addition to mesoscale inhomogeneities, aqueous solutions of certain hydrotropes, such as aqueous isobutyric acid, show a subtle "soap-like" third phase at the liquid–vapor interface.[49] The authors attributed the formation of this soap-like phase to the aggregation of solute molecules on the interface, driven by hydrophobic effects.

Motivated by this spectrum of explanations for the observed mesoscale inhomogeneities in aqueous solutions of hydrotropes, we set out to clarify this long-standing issue and carried out a systematic study of aqueous solutions of TBA. We

Published on 17 June 2013. Downloaded by National Institutes of Standards & Technology on 04/12/2013 20:37:51.

have combined results obtained from molecular dynamics (MD) simulations, small-angle neutron scattering (SANS) and dynamic light scattering (DLS) experiments to elucidate the nature and structure of these mesoscale inhomogeneities. We have studied aqueous solutions of TBA and aqueous solutions of TBA with cyclohexane (a typical hydrophobe with a molecular size similar to that of TBA). Since many of the mesoscale inhomogeneities reported in the literature did not appear to be at equilibrium (disappearing within several hours or days after sample preparation),[33,36] we paid special attention to long-term monitoring and equilibration of our samples. From MD simulations in TBA–water solutions, we see that TBA and water form short-lived (<1 nm in size), short-ranged (lifetime of tens of picoseconds) micelle-like structural fluctuations.[44] These structural fluctuations seem to be responsible for the anomalies in the thermodynamic properties of aqueous TBA solutions.[44] On the addition of a hydrophobic compound, larger aggregates of about 100 nm in size are formed as seen from DLS. These aggregates are not gaseous nanobubbles or solid particles but rather Brownian diffusive droplets. The aggregates consist of a hydrophobe-rich core surrounded by a hydrogen-bonded shell of hydrotrope and water molecules. They can be unusually stable over long periods of time (a year or longer).[39]

2 Materials and methods

2.1 Sample preparation

TBA was procured from two different sources: one (with a labeled purity greater than 99.7%) was purchased from Sigma Aldrich, while another (with a labeled purity greater than 99.8%) was purchased from Alfa-Aesar. Most of the samples described in this work were prepared by using the TBA procured from Alfa-Aesar, unless otherwise specified. Cyclohexane (CHX), with a labeled purity greater than 99%, was purchased from Merck. Heavy water (used for the SANS experiments), with a labeled purity greater than 99.9 atom%, was purchased from Sigma Aldrich. Deionized water was obtained from a Millipore setup.

For the DLS experiments, the binary TBA–water solutions were filtered with 200 nm Nylon filters to remove dust particles. In order to eliminate mesoscale inhomogeneities, additional cold filtrations with 20 nm Anopore filters (at a temperature of $\sim 5\ ^{\circ}C$), were carried out. CHX was used after filtering it through 200 nm Nylon filters. Light-scattering and neutron-scattering measurements were performed after equilibrating the samples for at least 24 h.

2.2 Molecular dynamics simulations

MD simulations on models for pure TBA, on TBA–water mixtures and TBA–water–CHX mixtures were performed. The concentration and number of molecules for each system are presented in Table 1. The TIP4P-Ew water model[50] was used and parameters for TBA and CHX were taken from the CHARMM General Force Field.[51] The systems were built by using the Packmol package,[52] which randomly packs all molecules in a simulation box.

The NAMD simulation program[53] was used to perform all MD simulations with 2 fs time steps for a total of 10 ns–1000 ns (see Table 1). Most simulations were run for 50 ns, while one binary TBA–water simulations was run longer to determine if any clathrate-like structures would form. The van der Waals interactions

 This journal is © The Royal Society of Chemistry 2013

Published on 17 June 2013. Downloaded by National Institutes of Standards & Technology on 04/12/2013 20:37:51.

Table 1 Concentrations of the samples studied by MD simulations

Sample #	TBA (mol%)	Water (mol%)	CHX (mol%)	T/K	Number of molecules	Time (ns)
Pure - P1	100	0	0	283	192	10
Binary						
B1	1	99	0	285	2125	50
B2	3.8	96.2	0	285	2188	1000
B3	7	93	0	285	2266	50
B4	18	82	0	285	2556	50
B5	40	60	0	285	3503	50
Ternary						
T1	11.84	85.31	2.84	298	8440	50
T2	17.70	79.65	2.65	298	9040	50
T3	27.78	69.44	2.78	298	8640	50
T4	40.05	57.21	2.74	298	8740	50

were smoothly switched off between 8 and 10 Å by a potential-based switching function. Long-range electrostatic interactions were calculated by using the particle-mesh Ewald (PME) method.[54] An interpolation order of 4 and a direct space tolerance of 10^{-6} were used for the PME method. Langevin dynamics were used to maintain constant temperatures for each system, while the Nosé-Hoover Langevin-piston algorithm[55,56] was used to maintain constant pressure at 1 bar. The Visual Molecular Dynamics (VMD) program[57] was used to create snapshots and to calculate the radial distribution functions (RDF).

2.3 Small-angle neutron scattering

SANS experiments were performed by using the NG3 SANS instrument at the NIST Center for Neutron Research. The SANS experiments were carried out on TBA–heavy water solutions and on TBA–heavy water–CHX solutions. The concentrations of the samples studied by SANS are presented in Table 2.

The essential measurement length scale in SANS is the wavenumber q. The wavenumber is related to the length scale l, as $l = 2\pi/q$, with $q = \left(\frac{4\pi}{\lambda}\right)\sin\left(\frac{\theta}{2}\right)$, where $\lambda = 6$ Å is the neutron wavelength, and θ is the scattering angle. In our experiments, q was varied from 0.005 $Å^{-1}$ to 0.5 $Å^{-1}$, corresponding to the length scales from ~1000 Å to ~10 Å.

Table 2 Concentrations of the samples studied by SANS and results from fits to eqn (4) and (5)

Sample #	TBA (mol %)	Heavy water (mol %)	CHX (mol %)	T/K	ξ_{OZ} (nm)	
Binary						
SB1	3.5	96.5	0	298	0.06	
SB2	5	95	0	298	0.24	
SB3	7.4	92.6	0	283	0.40	
				298	0.50	
				313	0.63	
Ternary						$R_{g(fixed)}$ (nm)
ST1	7.40	92.57	0.03	298	0.5	100

Published on 17 June 2013. Downloaded by National Institutes of Standards & Technology on 04/12/2013 20:37:51.

2.4 Dynamic light scattering

DLS experiments were performed with a PhotoCor Instruments setup, as described in ref. 37. Temperature was controlled with an accuracy of ±0.1 °C. For two exponentially decaying relaxation processes, the intensity auto-correlation function $g_2(t)$ (obtained in the homodyning mode) is given by:[58,59]

$$g_2(t) - 1 = \left[A_1 \exp\left(\frac{t}{\tau_1}\right) + A_2 \exp\left(\frac{t}{\tau_2}\right)\right]^2 \quad (1)$$

where A_1 and A_2 are the amplitudes of the two relaxation processes, t is the "lag" (or "delay") time of the photon correlations and τ_1 and τ_2 are the characteristic relaxation times. For a diffusive relaxation process, the decay rate (Γ) is related to the diffusion coefficient D, as:[58,59]

$$\Gamma = \frac{1}{\tau} = Dq^2 \quad (2)$$

where q is the difference in the wavenumber between incident and scattered light, $q = \left(\frac{4\pi n}{\lambda}\right)\sin\left(\frac{\theta}{2}\right)$, n is the refractive index of the solvent, λ is the wavelength of the incident light in vacuum ($\lambda = 633$ nm for our set-up), and θ is the scattering angle. For monodisperse, non-interacting, spherical Brownian droplets the hydrodynamic radius R can be calculated by using the Stokes–Einstein relation:[58,59]

$$R = \frac{k_B T}{6\pi\eta D} \quad (3)$$

where k_B is Boltzmann's constant, T is the temperature, and η is the shear viscosity of the medium.

3 Molecular-scale inhomogeneities

3.1 Phase behavior and thermodynamic anomalies of aqueous solutions of TBA

Fig. 1 shows the solid–liquid phase diagram of TBA–water solutions at ambient pressure.[60] While there exist different solid phases, the liquid phase is homogeneous on the macroscopic scale, with TBA and water completely miscible with each other. Fig. 1 also approximately shows the temperature and concentration domain (shaded in grey) where aqueous TBA solutions exhibit micelle-like structural fluctuations and thermodynamic anomalies. Excess and partial molar properties, heat capacity, and isothermal compressibility all exhibit extrema in the solvent-rich region of TBA–water solutions.[61–72] These anomalies occur in the concentration range of 3 mol% to 8 mol% (11 mass% to 26 mass%) TBA and become enhanced below room temperature.

The thermodynamic anomalies provide insight into solute–solvent interactions and on the structural changes that occur at the molecular scale. For example, as shown in Fig. 2, the enthalpy of mixing is negative in the solvent-rich region with a minimum at ~6 mol% (21 mass%) TBA, and becomes positive as the TBA concentration is increased.[66–68] The excess chemical potential of water shows a similar trend.[69,70] These anomalies indicate that at low TBA concentrations, solute–solvent interactions are favorable, with water and TBA molecules

 This journal is © The Royal Society of Chemistry 2013

Published on 17 June 2013. Downloaded by National Institutes of Standards & Technology on 04/12/2013 20:37:51.

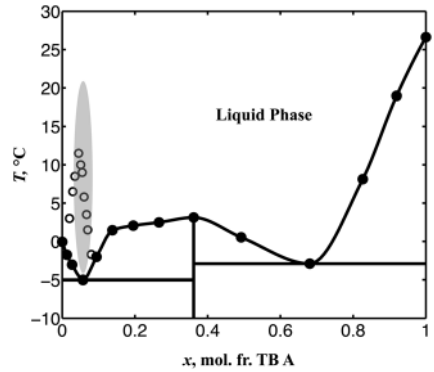

Fig. 1 Solid–liquid phase diagram of TBA–water solutions at ambient pressure (the solidus data points (connected by a guide to the eye) are reproduced with permission from ref. 59). The solid phase shows the presence of two eutectics (at ~6 mol% (21 mass%) and 70 mol% (90 mass%) TBA), while the liquid phase is macroscopically homogeneous. Open circles correspond to maxima of the heat capacity.[71] The grey area schematically represents the region where molecular scale clustering and thermodynamic anomalies are reported. Mesoscale solubilization of hydrophobic compounds is also observed in this region. The horizontal and vertical black lines separate the different phases of TBA–water hydrates.

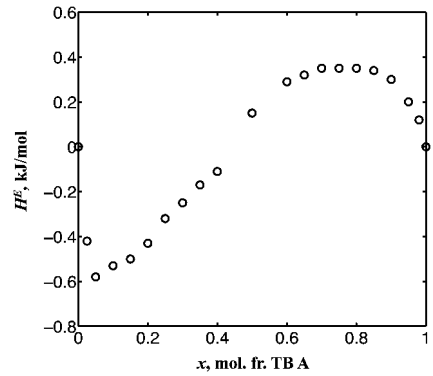

Fig. 2 Excess enthalpy (heat of mixing) of aqueous TBA solutions at $T = 25$ °C (reproduced with permission from ref. 67). The negative values of the excess enthalpy in the water rich region indicate favorable solute–solvent interactions.

preferring to couple with each other. As the TBA concentration is increased, solute–solute and solvent–solvent interactions are favored over solute–solvent interactions, indicating that TBA and water molecules prefer to demix.

The heat capacity of aqueous TBA solutions also exhibits anomalies, with maxima observed in the solute-rich region.[64,65] The maxima become sharper as the temperature is lowered.[72] This could be an indication of a structural change in this region. Remarkably, as most recent experiments have demonstrated, this heat capacity anomaly is rather insensitive to the presence or absence of mesoscale inhomogeneities (the heat capacity anomaly persists even after the mesoscale inhomogeneities have been eliminated by filtration).[73] This indicates that the anomaly is inherent to the molecular structure of binary TBA–water solutions,

Published on 17 June 2013. Downloaded by National Institutes of Standards & Technology on 04/12/2013 20:37:51.

and is not significantly affected by the presence (or absence) of mesoscale inhomogeneities.

Thermodynamic anomalies have also been observed in aqueous solutions of many other hydrotropes. Aqueous solutions of other alcohols such as methanol, ethanol, *n*-propanol, isopropanol, and 2-butoxyethanol all show similar anomalies in their thermodynamic properties within the water-rich region.[1] In TBA–water solutions, these anomalies are most pronounced.[1] We attribute these thermodynamic anomalies, to structural fluctuations (clustering) occurring on the molecular scale.[44] MD simulations of TBA–water solutions, presented in the following section, support this view.

3.2 Molecular-scale clustering in aqueous solutions of TBA

MD simulations were performed on models of pure TBA and aqueous solutions of TBA. In the aqueous solutions, the concentration of TBA was varied from 1 mol% to 40 mol% (4 mass% to 73 mass%). Fig. 3a shows the radial distribution functions (RDFs) between the central carbons of TBA in pure TBA and in aqueous solutions of TBA. In pure TBA, there exists a peak at a distance of 4.7 Å and a second peak at a distance of 6 Å. The first peak in the RDF corresponds to strong

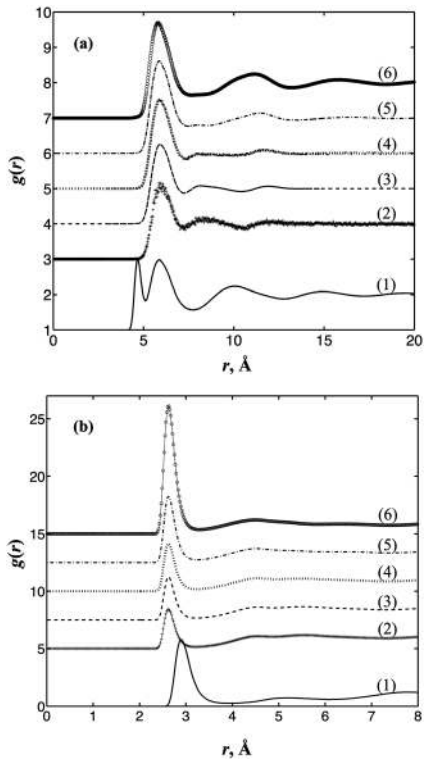

Fig. 3 Radial distribution functions between: (a) Central carbons of TBA and (b) oxygen of TBA and oxygen of water (for pure TBA RDF is between oxygen atoms of TBA). The curves are offset vertically for clarity. (1) Pure TBA. (2) 1 mol% (4 mass%) TBA. (3) 4 mol% (15 mass%) TBA. (4) 7 mol% (24 mass%) TBA. (5) 18 mol% (47 mass%) TBA. (6) 40 mol% (73 mass%) TBA.

 This journal is © The Royal Society of Chemistry 2013

Published on 17 June 2013. Downloaded by National Institutes of Standards & Technology on 04/12/2013 20:37:51.

van der Waals interactions, while the second peak corresponds to weaker van der Waals interactions, between the methyl groups of TBA.

In the aqueous solutions, the first peak (at 4.7 Å) between the central C atoms of TBA disappears, but the peak at 6 Å becomes enhanced. This indicates that in aqueous solutions, TBA molecules prefer to interact with water rather than with other TBA molecules, in agreement with thermodynamic anomalies. It is also observed that the magnitude of this peak increases as the TBA concentration is increased. This is an indication that at higher TBA concentrations more TBA molecules "cluster" together at this distance. Secondary and tertiary peaks are also seen in aqueous TBA solutions, which differs from simulations of pure TBA. As the concentration of TBA increases, the secondary peak occurring at 8 Å tends to disappear. This could be an indication that at higher concentrations aqueous TBA solutions do not form "isolated clusters" with water or that the clustering with water has changed in a TBA-rich solution.

Fig. 3b shows the RDFs between the oxygen atom of TBA and the oxygen atom of water in aqueous solutions of TBA and between oxygen atoms of TBA in the pure TBA system. This figure shows a large initial peak at 3 Å in pure TBA, which disappears in aqueous solutions. An initial peak between water and TBA is seen in aqueous solutions at 2.6 Å. This again indicates that in aqueous solutions, TBA tends to form hydrogen bonds with water rather than with itself. Moreover, the distance is shorter indicating stronger hydrogen bond with water than between TBA–TBA. As the concentration of TBA increases, the magnitude of the first peak increases. This indicates that there is a stronger preference for water to form a hydrogen bond with the hydroxyl of TBA at these higher concentrations. As the TBA concentration is raised, the secondary peak, which occurs at 4.4 Å, increases while the tertiary and higher peaks almost disappear. This indicates that at higher TBA concentrations the water molecules surrounding the TBA molecules in tertiary shells and beyond are not very well defined and the resultant "cluster" loses its structural integrity.

Snapshots from MD simulations can help in interpreting the RDFs as shown in Fig. 4. At the lower concentrations, TBA forms clusters due to van der Waals interactions between its methyl groups. These TBA clusters are surrounded by a hydrogen-bonded polygonal (either pentagonal (Fig. 4b and c) or hexagonal (not shown)) network formed between TBA–water and water–water molecules. The main RDF peak at 6 Å, as seen in Fig. 3a, corresponds to the distance between central carbon atoms of TBA, which may be dimers, trimers or tetramers of TBA. The secondary peak at 8 Å, as seen in Fig. 3a, corresponds to a distance between the central carbon atoms in oligomerized TBA with its nearest neighbor of unstructured TBA. The water molecules are organized in a specific hydrogen-bonded structure around TBA molecules, with the hydroxyl group of the TBA molecules forming one of the vertices of a hydrogen-bonded polygon.

The structural significance of the peaks calculated in the O(TBA)–O(Water) RDFs of Fig. 3b can be visualized from the snapshots in Fig. 4. The primary peak in Fig. 3b is from 3 waters coordinating the hydroxyl group of TBA. The secondary RDF peak at 4.4 Å and the tertiary peak at 5.6 Å in Fig. 3b correspond to larger distances between the vertices in the pentagon and/or hexagon ring of water. The secondary and tertiary peaks correspond to an additional 17 to 21 surrounding water molecules. This leads to an effective structure, which we refer to as a "micelle-like cluster". The cluster has an inner radius of $\sim$4 Å that constitutes 4 to

Published on 17 June 2013. Downloaded by National Institutes of Standards & Technology on 04/12/2013 20:37:51.

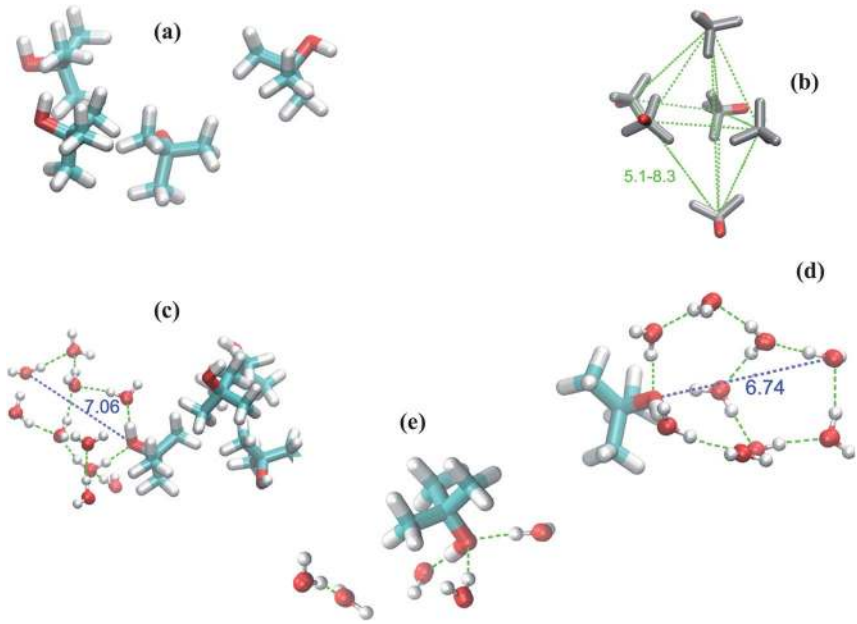

Fig. 4 Snapshots from MD simulations in aqueous solutions of TBA with increasing concentration of TBA. TBA molecules are represented by the licorice model, while water molecules are represented by the ball and stick model. The structure between TBA and water is fairly similar from 1 mol% to 7 mol% TBA. The only difference is the amount and size of TBA clusters with increasing TBA concentration. However, beyond ~7 mol% TBA, the clusters do not seem to be well-defined and lose their structural integrity. (a) 1 mol% (4 mass%) TBA. (b) 4 mol% (15 mass%) TBA. (c) 7 mol% (24 mass%) TBA. (d) 18 mol% (47 mass%) TBA. (e) 40 mol% (73 mass%) TBA.

5 TBAs and an additional distance, including water shells, of ~6.5 Å. Thus, this "micelle-like cluster" constituting TBA and water molecules is ~10.5 Å in radius. Although the water structures surrounding TBA form polygons commonly found in hydrates,[74] the micelle-like clusters are short-lived and appear to be transient, with an estimated lifetime of the order of 10 ps–50 ps.

The effect of TBA concentration seen from the RDFs of aqueous TBA solutions can also be explained from the snapshots in Fig. 4. At low concentrations, 1 mol% to 2 mol% (4 mass% to 8 mass%) TBA, the average cluster sizes of TBA molecules range from 1 to 4 and the number of clusters tends to be small. TBA forms a micelle-like cluster with water. At higher TBA concentrations, 3 mol% to 7 mol% (11 mass% to 24 mass% TBA), the clusters tend to be larger with 4–8 TBA molecules. Bipyramidal structures of TBA clusters (Fig. 4b) transiently exist (20 ps to 50 ps) in the 3 mol% to 7 mol% concentration range. As the TBA concentration is further raised, the clusters of TBA–water do not behave as a micelle, but rather TBA becomes dominant in terms of volume component in the solution (Fig. 5d and e), reflecting a growing tendency to be apart from water molecules. These solutions no longer have the short-lived TBA–water clusters and instead look more like a randomly mixed solution of TBA and water (usual non-ideal solution). At 40 mol% (73 mass%) TBA, the water concentration is too low to form any significant water polygon structure indicative of the reduction and loss of secondary and higher order peaks in the RDFs (Fig. 3).

 This journal is © The Royal Society of Chemistry 2013

Published on 17 June 2013. Downloaded by National Institutes of Standards & Technology on 04/12/2013 20:37:51.

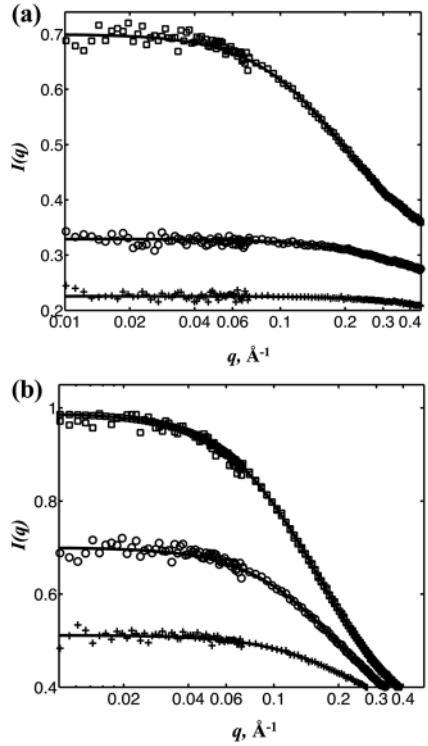

Fig. 5 (a) SANS data from TBA–heavy water solutions at $T = 25$ °C. Crosses: 3.5 mol% (12 mass%) TBA (sample # SB1). Circles: 5 mol% (16 mass%) TBA (sample # SB2). Squares: 7.4 mol% (23 mass%) TBA (sample # SB3). Standard statistical error bars are comparable to the size of the symbols. The solid lines are fits to the data in accordance with eqn (4). The results of the fits are summarized in Table 2. (b) SANS data from a 7.4 mol% (23 mass%) TBA–heavy water solution (sample # SB3). Crosses: 10 °C. Circles: 25 °C. Squares: 40 °C. Standard statistical error bars are comparable to the size of the symbols. The black lines are fits to the data in accordance with eqn (4). The results of the fits are summarized in Table 2.

3.3 SANS in aqueous solutions of TBA

In order to characterize the molecular-scale inhomogeneities in aqueous solutions of TBA, SANS experiments were carried out on TBA–heavy water solutions. The following equation best fits the SANS intensity data:[71]

$$I(q) = \frac{A_3}{1 + (\xi q)^2} + B \tag{4}$$

where A_3 is the amplitude, B is a background parameter, and ξ is the correlation length, which characterizes the length scale of concentration fluctuations; it increases as the temperature is raised and as the TBA concentration is increased. This behavior of the correlation length is expected as the system approaches a "virtual" critical point (hidden here by the vapor–liquid transition, but may become real on the addition of a salt, such as KCl[27]) located at an inaccessible higher temperature and higher TBA concentration. Fig. 5a shows the SANS data for various concentrations of TBA at 25 °C, while Fig. 5b shows the SANS data for 7.4 mol% (23 mass%) TBA solution at different temperatures. The results from

Published on 17 June 2013. Downloaded by National Institutes of Standards & Technology on 04/12/2013 20:37:51.

the SANS fits are presented in Table 2. The results obtained for the correlation length are consistent with what has been observed in the literature.[27]

We also wanted to investigate whether the micelle-like clusters (structural fluctuations) observed from MD simulations could be seen from SANS data. However, we were unable to unambiguously detect such clusters, although some spectra at low temperatures suggest the existence of a marginally detectable peak in the structure factor at $q \sim 0.1$ Å. The reasons for this could be two-fold: poor SANS contrast between these clusters and the bulk solution or small contribution of these clusters into the intensity as compared to the contribution from the concentration fluctuations.

4 Mesoscale inhomogeneities

4.1 DLS and SANS in aqueous solutions of TBA upon the addition of a hydrophobe

The discussion so far has focused on molecular-scale (order of 1 nm in size) inhomogeneities in aqueous TBA solutions. However as mentioned earlier, there have been many reports on the existence of mesoscale inhomogeneities (order of 100 nm in size) in aqueous solutions of TBA.[22–38] We have carried out a comprehensive experimental study to elucidate their origin and to characterize these mesoscale inhomogeneities.[37–39]

Fig. 6 shows the intensity auto-correlation function observed from an aqueous solution of TBA (purchased from Sigma Aldrich). The correlation function shows the presence of two relaxation processes – a fast process with a relaxation time of 65 μs and a slow process with a relaxation time of 22 ms. The fast process corresponds to molecular diffusion, with a diffusion coefficient of 1.5×10^{-6} cm^2 s^{-1}. In accordance with eqn (3), this corresponds to a hydrodynamic radius of

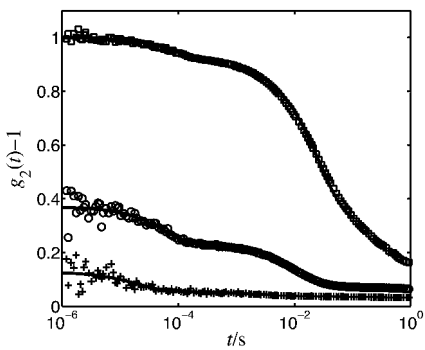

Fig. 6 Time-dependent intensity autocorrelation functions obtained in aqueous solutions of TBA from dynamic light scattering ($\theta = 45°$). The solid lines are fits to the data in accordance with eqn (1). Circles represent the correlation function obtained in ~8 mol% (26 mass%) TBA solution (TBA procured from Sigma Aldrich) at $T = 24$ °C. This correlation function shows the presence of two relaxation modes – the fast mode with a relaxation time of ~65 μs and a slow mode with a relaxation time of ~22 ms. After filtering this solution multiple times with a 20 nm Anopore filter at ~10 °C, the slow mode is almost eliminated (correlation function represented by crosses). Adding trace amounts of a hydrophobic component (0.03 mol% cyclohexane) regenerates the slow mode (correlation function represented by squares). Statistical error bars are comparable to the size of the symbols.

 This journal is © The Royal Society of Chemistry 2013

Published on 17 June 2013. Downloaded by National Institutes of Standards & Technology on 04/12/2013 20:37:51.

about 0.6 nm. This is consistent with the correlation length (ξ) of the concentration fluctuations obtained from SANS data as discussed in the previous section.

The slower process, with a relaxation time of 22 ms, corresponds to mesoscale inhomogeneities.[37] As the temperature is increased, this slow mode disappears and reappears as the temperature is lowered.[37] In fact, at low temperatures the contribution from the slow mode is enhanced so significantly, that it becomes quite difficult to detect molecular diffusion.[37] The mesoscale inhomogeneities were only observed between the concentrations 3 mol% to 8 mol% (11 mass% to 26 mass%) TBA. Above this concentration range, the mesoscale inhomogeneities disappeared.

In order to understand the origin of the slow mode, this aqueous TBA solution was filtered multiple times by using a 20 nm Anopore filter, at a low temperature ($\sim$5 °C), to eliminate the slow mode. The intensity auto-correlation function obtained after filtering the aqueous TBA solutions at cold conditions is also shown in Fig. 6. The resultant correlation function shows no mesoscale inhomogeneities, but only the contribution from molecular diffusion. A controlled "impurity", namely a trace amount (0.03 mol%) of a third, more hydrophobic, component (cyclohexane) was added to an aqueous TBA solution that initially did not show any mesoscale inhomogeneities. Upon the addition of cyclohexane, mesoscale inhomogeneities emerged, and the slow mode was observed. Various hydrophobic additives such as propylene oxide, isobutyl alcohol, and methyl *tert*-butyl ether were also studied. All these experiments showed that the slow mode appears only when the aqueous TBA solution contains a more hydrophobic component.[38] The wavenumber dependence of the relaxation rate of these inhomogeneities (in accordance with eqn (2)) revealed that they are diffusive Brownian droplets.[38] Confocal microscopy images are also consistent with what is observed from dynamic light scattering.[37]

The presence of mesoscopic droplets can also be verified from SANS experiments. Fig. 7 shows the SANS intensity $I(q)$ from a TBA–heavy water solution containing trace amounts of cyclohexane (CHX) as the hydrophobe. The SANS

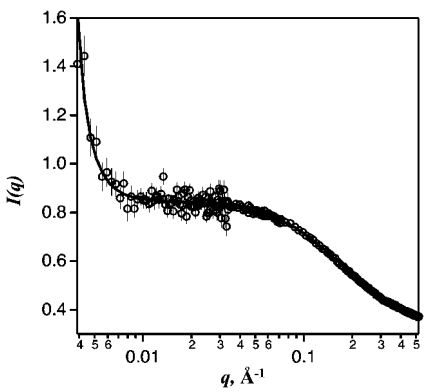

Fig. 7 SANS data from a TBA–heavy water–CHX solution at $T = 25$ °C. 7.4 mol% TBA (23 mass%), 0.03 mol% (0.1 mass%) CHX (sample # ST1 from Table 2). The black line is a fit to the data in accordance with eqn (5). The results of the fit are summarized in Table 2. Statistical error bars represent one standard deviation.

Published on 17 June 2013. Downloaded by National Institutes of Standards & Technology on 04/12/2013 20:37:51.

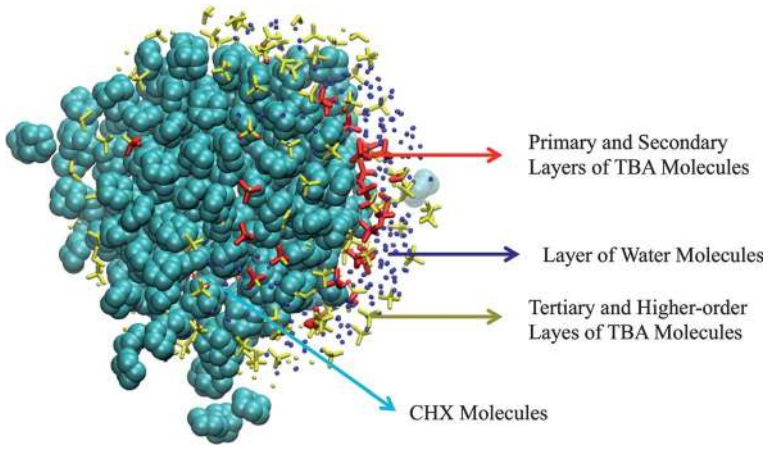

Fig. 8 Snapshots (at ~50 ns) from MD simulations of a TBA–water–CHX solution (sample # T1 from Table 1). TBA molecules are represented by the licorice model, while van der Waals spheres represent CHX molecules. This snapshot demonstrates the formation of a "droplet" with aggregated CHX molecules in the core, surrounded by primary and secondary layers of TBA molecules. These layers are further solvated by a water layer and a tertiary layer of TBA molecules.

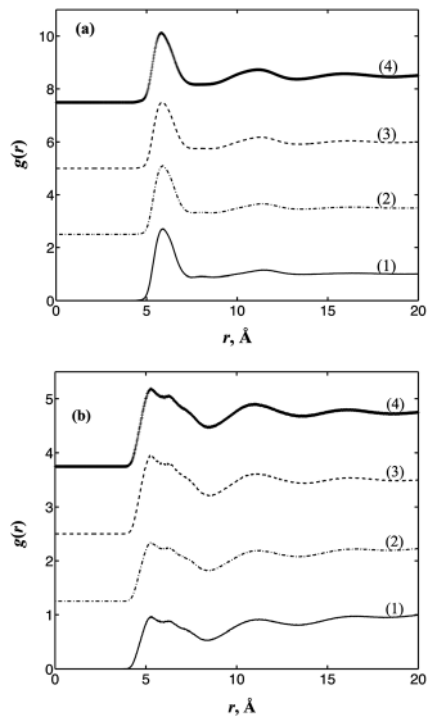

Fig. 9 Radial distribution functions in TBA–water–CHX solutions with increasing concentrations of TBA (samples # T1 to T4 from Table 1). (a) RDFs between central C atoms of TBA (b) RDFs between central C of TBA and C1 on CHX.

 This journal is © The Royal Society of Chemistry 2013

Published on 17 June 2013. Downloaded by National Institutes of Standards & Technology on 04/12/2013 20:37:51.

data in this TBA–heavy water–CHX system were best fit to an equation of the following form:[75]

$$I(q) = \frac{A_4}{(R_g q)^4} + \frac{A_5}{1 + (\xi q)^2} + B_1 \quad (5)$$

where A_4 and A_5 are the amplitudes, R_g is the radius of gyration of the mesoscopic droplets, ξ is the correlation length of the concentration fluctuations, and B_1 is a background parameter. The above equation includes contributions from the concentration fluctuations and contributions from the much larger, mesoscopic droplets. Since the SANS data do not reach a Guinier region (plateau at low q), the R_g corresponding to mesoscopic droplets was fixed at 100 nm (as was observed from DLS).

4.2 Investigating the structure of mesoscopic droplets by MD simulations

In order to further investigate the nature of these mesoscopic droplets, MD simulations of TBA–water–CHX solutions were carried out. Fig. 8 shows a snapshot from MD simulations where aggregated CHX molecules are surrounded by TBA molecules. The concentration of TBA in the layer surrounding the CHX aggregate is higher than in the bulk solution. The structure of this layer is similar to a "microemulsion" structure, which seems to occur at higher concentrations of TBA.[20] Water molecules form hydrogen bonds with the hydroxyl groups of the TBA molecules. There may be secondary or higher order layers of TBA and water molecules that surround the CHX aggregate (Fig. 8), leading to the formation of a "droplet". The observed droplets remained stable for the length of the simulation.

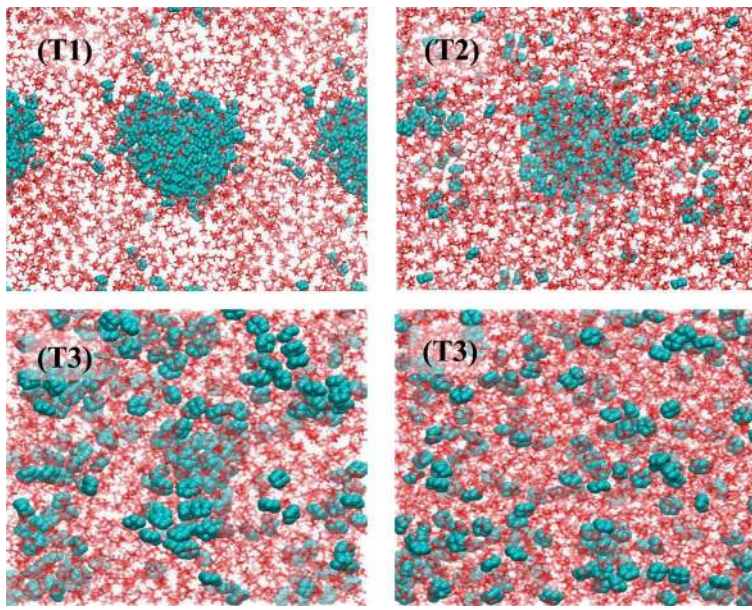

Fig. 10 Snapshots from MD simulations in TBA–water–CHX system with increasing concentrations of TBA (samples # T1 to T4 from Table 1). These snapshots indicate that as the TBA concentration increases, the tendency of CHX to form droplets decreases. At high TBA concentrations, TBA and CHX preferred to remain mixed, rather than form the droplets.

Published on 17 June 2013. Downloaded by National Institutes of Standards & Technology on 04/12/2013 20:37:51.

Simulations of TBA–water–CHX solutions with different concentrations of TBA, but almost the same concentration of CHX, were also carried out. Fig. 9a shows the RDFs between central carbon atoms of TBA molecules, while Fig. 9b shows the RDFs between central C of TBA molecule and a carbon on the CHX (C1) molecule. Fig. 10a to d show snapshots from MD simulations. The RDFs and the snapshots indicate that as the TBA concentration increases, the tendency to form "droplets" (as described above) disappears. Fig. 10c and d show that at high TBA concentrations, TBA and CHX prefer to remain mixed with each other rather than form droplets.

5 Mesoscale solubilization – a state between molecular solubility and macrophase separation

We refer to the phenomenon of formation of mesoscopic droplets in aqueous solutions of hydrotropes containing hydrophobes, as the mesoscale solubilization. Mesoscale solubilization is a distinct intermediate state between molecular solubility and macrophase separation.[76] Molecular solubility of nonpolar solutes (hydrophobes) in water can be explained by the phenomenon of hydrophobic hydration,[77–79] where water molecules form a hydrogen-bonded shell around the solute molecule. This shell is similar to a clathrate shell and the water molecules in the shell do not interact strongly with the nonpolar solute in the core.[79] However, molecular solubility in aqueous solutions of nonionic hydrotropes is quite different, where the water molecules strongly interact with the solute molecules through strong hydrogen bonds. This interaction leads to the formation of loose micelle-like clusters in water–hydrotrope solutions. Such clusters may have the same length scale as the correlation length of the concentration fluctuations (when far away from the critical point), but very different dynamics. Clusters, which have a life-time of tens of picoseconds, relax by the reorientation of hydrogen bonds, while concentration fluctuations have a time-scale of about tens of microseconds at $q \sim 10^7$ m^{-1} (when far away from the critical point) and relax by diffusion. The cluster dynamics can be experimentally detected by dynamic neutron scattering techniques such as disc chopper spectrometer (DCS) or neutron spin echo (NSE), whereas concentration fluctuations can be detected by both SANS and DLS.

On the addition of a hydrophobe (such as cyclohexane), the short-lived micelle-like clusters that originally exist in hydrotrope-water binary solutions (such as in TBA–water) seem to be stabilized and rearranged. Over a certain concentration range of hydrophobe, the hydrophobe molecules start to aggregate. Part of the hydrotrope–water clusters surround the hydrophobe aggregates, protecting them from the water-rich environment. Thus, we view the mesoscopic droplets as having a hydrophobe-rich core, surrounded by a hydrogen-bonded "micro-emulsion-like" water–hydrotrope shell. The schematic of such a droplet is shown in Fig. 11. This picture is consistent with what has been observed and interpreted in other aqueous systems.[22,80]

In order to understand the thermodynamic stability of the mesoscopic droplets, we have studied the macroscopic behavior of the ternary system TBA–water–CHX.[76] The ternary phase diagram at ambient conditions is shown in Fig. 12.[76] This figure shows that TBA is completely miscible with water and CHX, while water and CHX are almost completely immiscible with each other. The region

 This journal is © The Royal Society of Chemistry 2013

Published on 17 June 2013. Downloaded by National Institutes of Standards & Technology on 04/12/2013 20:37:51.

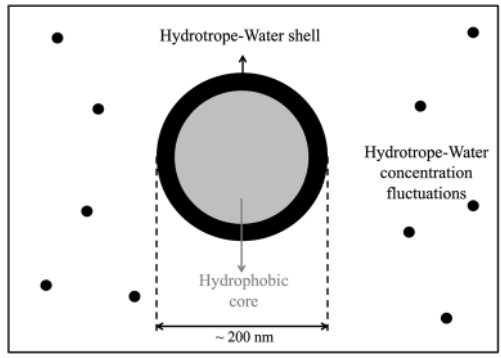

Fig. 11 Schematic representation of mesoscale solubilization in aqueous solutions of hydrotropes containing a hydrophobe. The mesoscopic droplets have a hydrophobic core surrounded by a hydrogen-bonded microemulsion-like hydrotrope–water shell.

where mesoscopic droplets are observed is shown in the inset of Fig. 12. Remarkably, this region corresponds to the concentration range where structural fluctuations and thermodynamic anomalies are observed in binary TBA–water solutions. Mesoscopic droplets are not observed on the addition of CHX to pure water or to TBA–water solutions where the TBA concentration is greater than 25 mol%. In the region around 7 mol% TBA the mesoscale droplets are extremely long-lived, being stable for over a year.[39] Only in the presence of a macroscopic hydrophobe-rich phase (samples studied in the two-phase region of the ternary

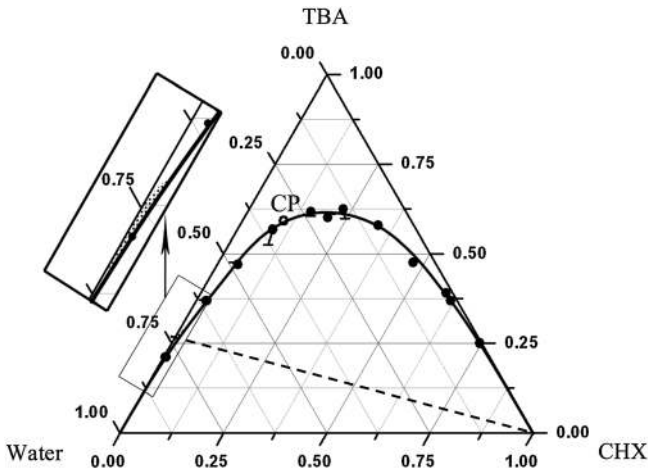

Fig. 12 Phase diagram of TBA–water–CHX system at $T = 21$ °C (reproduced from ref. 39). The smooth line across the points is a guide to the eye. All concentrations are shown as mass fractions. The open circle (CP) represents the approximate location of the critical point. The dashed line from the vertex of the hydrophobe (CHX) represents concentrations with a constant TBA–water ratio (25 : 75 mass basis/7 : 93 mole basis) where thermodynamic anomalies in the binary TBA–water solution are observed. The region inside the solid curve is the two-phase region, while the region outside this curve is the macroscopic one-phase region. The dotted area in the phase diagram shows the region where mesoscopic droplets are observed.

Published on 17 June 2013. Downloaded by National Institutes of Standards & Technology on 04/12/2013 20:37:51.

system), these droplets tend to slowly (over a period of months) condense on the water–CHX interface. The instability of the mesoscopic droplets in the presence of the macroscopic water–CHX interface may be due to the destruction of the TBA–water protective shell, which surrounds the hydrophobic CHX core.

Mesoscale solubilization, being intermediate between molecular solubility and macroscopic phase separation, makes the traditional definition of solubility ambiguous. Thus, popular experimental techniques, such as chromatography methods, used for measuring solubility of hydrophobic species in water may be misinterpreted. Moreover, the bulk equilibration may require an unrealistically long time, making the definition of thermodynamic equilibrium also ambiguous.

6 Summary and conclusions

We have investigated molecular-scale and mesoscale inhomogeneities in TBA–water solutions and in TBA–water–CHX solutions. We have combined results obtained from MD simulations with those obtained from SANS and DLS experiments. MD simulations in TBA–water solutions show the presence of short-ranged ($\sim$1 nm), short-lived (10 ps–50 ps) clusters, interpreted as micelle-like structural fluctuations. These clusters may have a length-scale similar to the concentration fluctuations, but have very different (much faster) dynamics. Concentration fluctuations relax by diffusion, while clusters relax by the reorientation of hydrogen bonds. Clustering is observed in the low concentration region of TBA (1 mol% to 8 mol% or 4 mass% to 26 mass%) and tends to disappear at higher TBA concentrations. These clusters are likely responsible for the thermodynamic anomalies observed in aqueous TBA solutions. We were unable to unambiguously detect these clusters from SANS experiments, but the presence of concentration fluctuations was clearly detected by both SANS and DLS techniques.

Mesoscale inhomogeneities, which are Brownian diffusive droplets, order of 100 nm in size, are observed in aqueous solutions of TBA containing a hydrophobic component. The hydrophobe tends to stabilize and rearrange the short-ranged, short-lived structural fluctuations initially present in aqueous TBA solutions and leads to the formation of larger (mesoscopic) droplets. The structure of these droplets is such that they contain a hydrophobe-rich core surrounded by a microemulsion-like hydrogen-bonded shell of TBA and water molecules. The shell can be regarded as a "protective layer" consisting of TBA and water molecules, which separate the oily core of the aggregates from the aqueous-rich bulk phase of the solution. We call the formation of mesoscopic droplets in aqueous solutions of hydrotropes, containing hydrophobe, the mesoscale solubilization.

Two peculiar features characterize mesoscale solubilization. The mesoscopic droplets are order of 100 nm in size. This size does not seem to significantly depend on the type of the hydrotrope or the hydrophobe. Lowering the temperature enhances the number of these droplets, but their size remains almost unchanged. Moreover, these droplets are extremely long-lived, being stable for over a year. Only in the presence of a macroscopic hydrophobe-rich phase do these droplets tend to slowly (over a period of months) condense on the water–oil interface. The phenomenon observed in aqueous solutions of TBA may represent a ubiquitous feature of aqueous solutions of nonionic hydrotropes, and may have important practical implications in areas such as drug delivery, where traditional surfactants may need to be replaced by hydrotropes.

 This journal is © The Royal Society of Chemistry 2013

Published on 17 June 2013. Downloaded by National Institutes of Standards & Technology on 04/12/2013 20:37:51.

Acknowledgements

We acknowledge fruitful discussions with J. Leys and V. Molinero. We also thank J. V. Sengers for useful comments on the manuscript. This research is supported by the Division of Chemistry of the National Science Foundation under Grant No. CHE-1012052 (MAA). Part of this research (MD simulations) was supported by the National Science Foundation through XSEDE resources provided by National Institute for Computational Sciences under grant number TG-MCB100139 (JBK). Additional computational resources were used on the High Performance Computing Cluster at the University of Maryland. SANS work is based upon activities supported by the National Science Foundation under Agreement No. DMR-0944772. The identification of commercial products does not imply endorsement by the National Institute of Standards and Technology nor does it imply that these are the best for the purpose.

References

1 F. Franks and D. G. Ives, The structural properties of alcohol-water mixtures, *Q. Rev. Chem. Soc.*, 1966, **20**, 1–44.
2 F. Franks, *Water: A Comprehensive Treatise*, Volumes 2 and 7, Plenum Press, New York, 1982.
3 G. D'Arrigo and J. Teixeira, Small-angle neutron scattering study of D_2O-alcohol solutions, *J. Chem. Soc., Faraday Trans.*, 1990, **86**, 1503–1509.
4 G. D'Arrigo, R. Giordano and J. Teixeira, Temperature and concentration dependence of SANS spectra of aqueous solutions of short-chain amphiphiles, *Eur. Phys. J. E*, 2009, **29**, 37–43.
5 M. Misawa, T. Sato, A. Onozuka, K. Maruyama, K. Mori, S. Suzuki and T. Otomo, A visualized analysis of small-angle neutron scattering intensity: Concentration fluctuation in alcohol-water mixtures, *J. Appl. Crystallogr.*, 2007, **40**, s93–s96.
6 R. D. Koehler, K.-V. Schubert, R. Strey and E. W. Kaler, The Lifshitz line in binary systems: Structures in water/C_4E1 mixtures, *J. Chem. Phys.*, 1994, **101**, 10843–10849.
7 K. Yoshida, T. Yamaguchi, T. Otomo, M. Nagao, H. Seto and T. Takeda, Concentration fluctuations and cluster dynamics of 2-butoxyethanol-water mixtures by small-angle neutron scattering and neutron spin echo techniques, *J. Mol. Liq.*, 2005, **119**, 125–131.
8 J. L. Finney, D. T. Bowron and A. K. Soper, The structure of aqueous solutions of tertiary butanol, *J. Phys.: Condens. Matter*, 2000, **12**, A123–A128.
9 D. T. Bowron, J. L. Finney and A. K. Soper, Structural investigation of solute-solute interactions in aqueous solutions of tertiary butanol, *J. Phys. Chem. B*, 1998, **102**, 3551–3563.
10 J. L. Finney, D. T. Bowron, R. M. Daniel, P. A. Timmins and M. A. Roberts, Molecular and mesoscale structures in hydrophobically driven aqueous solutions, *Biophys. Chem.*, 2003, **105**, 391–409.
11 D. T. Bowron, J. L. Finney and A. K. Soper, Structural characteristics of a 0.23 mole fraction aqueous solution of tetrahydrofuran at 25 °C, *J. Phys. Chem. B*, 2006, **110**, 20235–20245.
12 K. R. Harris and P. J. Newitt, Diffusion and structure in water-alcohol mixtures: Water + *tert*-butyl alcohol (2-methyl-2-propanol), *J. Phys. Chem. A*, 1999, **103**, 6508–6513.
13 N. Nishi, S. Takahashi, M. Matsumoto, A. Tanaka, K. Muraya, T. Takamuku and T. Yamaguchi, Hydrogen bonding cluster formation and hydrophobic solute association in aqueous solution of ethanol, *J. Phys. Chem.*, 1995, **99**, 462–468.
14 P. G. Kusalik, A. P. Lyubartsev, D. L. Bergman and A. Laaksonen, Computer simulation study of *tert*-butyl alcohol. 2. Structure in aqueous solution, *J. Phys. Chem. B*, 2000, **104**, 9533–9539.
15 J.-H. Guo, Y. Luo, A. Augustsson, S. Kashtanov, J.-E. Rubensson, D. K. Shuh, H. Ågren and J. Nordgren, Molecular structure of alcohol-water mixtures, *Phys. Rev. Lett.*, 2003, **91**, 157401.
16 A. Fornili, M. Civera, M. Sironi and S. L. Fornili, Molecular dynamics simulation of aqueous solutions of trimethylamine-N-oxide and *tert*-butyl alcohol, *Phys. Chem. Chem. Phys.*, 2003, **5**, 4905–4910.

Published on 17 June 2013. Downloaded by National Institutes of Standards & Technology on 04/12/2013 20:37:51.

17 M. Kiselev and I. Ivlev, The study of hydrophobicity in water-methanol and water-*tert*-butanol mixtures, *J. Mol. Liq.*, 2004, **110**, 193–199.
18 A. B. Roney, B. Space, E. W. Castner, R. L. Napoleon and P. B. Moore, A molecular dynamics study of the aggregation phenomena in aqueous *n*-propanol, *J. Phys. Chem. B*, 2004, **108**, 7389–7401.
19 S. K. Allison, J. P. Fox, R. Hargreaves and S. P. Bates, Clustering and microimmiscibilityin alcohol-water mixtures: Evidence from molecular-dynamics simulations, *Phys. Rev. B*, 2005, **71**, 024201.
20 B. Kežić and A. Perera, Aqueous *tert*-butanol mixtures: A model for molecular emulsions, *J. Chem. Phys.*, 2012, **137**, 014501.
21 R. Gupta and G. N. Patey, Aggregation in dilute aqueous *tert*-butyl alcohol solutions: Insights from large-scale simulations, *J. Chem. Phys.*, 2012, **137**, 034509.
22 Z. Li, H. Cheng, J. Li, L. Hao, L. Zhang, B. Hammouda and C. C. Han, Large-scale structures in tetrahydrofuran-water mixture with a trace amount of antioxidant butylhydroxytoluene (BHT), *J. Phys. Chem. B*, 2011, **115**, 7887–7895.
23 M. F. Vuks and L. V. Shurupova, The scattering of light and phase transition in solutions of tertiary butyl alcohol in water, *Opt. Commun.*, 1972, **5**, 277–278.
24 C. W. Beer, Jr. and D. J. Jolly, Comments on "the scattering of light and phase transition in solutions of tertiary butyl alcohol in water", *Opt. Commun.*, 1974, **11**, 150–151.
25 K. Iwasaki and T. Fujiyama, Light scattering study of clathrate hydrate formation in binary mixtures of *tert*-butyl alcohol and water, *J. Phys. Chem.*, 1977, **81**, 1908–1912.
26 K. Iwasaki and T. Fujiyama, Light-scattering study of clathrate hydrate formation in binary mixtures of *tert*-butyl alcohol and water: 2. Temperature effect, *J. Phys. Chem.*, 1979, **83**, 463–468.
27 G. W. Euliss and C. M. Sorensen, Dynamic light scattering studies of concentration fluctuations in aqueous *t*-butyl alcohol solutions, *J. Chem. Phys.*, 1984, **80**, 4767–4773.
28 T. M. Bender and R. Pecora, A dynamic light scattering study of the *tert*-butyl alcohol-water system, *J. Phys. Chem.*, 1986, **90**, 1700–1706.
29 T. M. Bender and R. Pecora, Dynamic light scattering measurements of mutual diffusion coefficients of water-rich 2-butoxyethanol/water systems, *J. Phys. Chem.*, 1988, **92**, 1675–1677.
30 Y. Georgalis, A. M. Kierzek and W. Saenger, Cluster formation in aqueous electrolyte solutions observed by dynamic light scattering, *J. Phys. Chem. B*, 2000, **104**, 3405–3406.
31 C. Yang, W. Lei and C. Wu, Laser light-scattering study of solution dynamics of water/cycloether mixtures, *J. Phys. Chem. B*, 2004, **108**, 11866–11870.
32 M. Sedlák, Large-scale supramolecular structure in solutions of low molar mass compounds and mixtures of liquids: I. Light scattering characterization, *J. Phys. Chem. B*, 2006, **110**, 4329–4338.
33 M. Sedlák, Large-scale supramolecular structure in solutions of low molar mass compounds and mixtures of liquids: II. Kinetics of the formation and long-time stability, *J. Phys. Chem. B*, 2006, **110**, 4339–4345.
34 M. Sedlák, Large-scale supramolecular structure in solutions of low molar mass compounds and mixtures of liquids: III. Correlation with molecular properties and interactions, *J. Phys. Chem. B*, 2006, **110**, 13976–13984.
35 F. Jin, X. Ye and C. Wu, Observation of kinetic and structural scalings during slow coalescence of nanobubbles in an aqueous solution, *J. Phys. Chem. B*, 2007, **111**, 13143–13146.
36 A. F. Kostko, M. A. Anisimov and J. V. Sengers, Criticality in aqueous solutions of 3-methyl pyridine and sodium bromide, *Phys. Rev. E*, 2004, **70**, 026118.
37 D. Subramanian, D. A. Ivanov, I. K. Yudin, M. A. Anisimov and J. V. Sengers, Mesoscale inhomogeneities in aqueous solutions of 3-methylpyridne and tertiary butyl alcohol, *J. Chem. Eng. Data*, 2011, **56**, 1238–1248.
38 D. Subramanian and M. A. Anisimov, Resolving the mystery of aqueous solutions of tertiary butyl alcohol, *J. Phys. Chem. B*, 2011, **115**, 9179–9183.
39 D. Subramanian, *Ph.D Dissertation*, University of Maryland, 2012.
40 C. Neuberg, Hydrotropische erscheinungen, *Biochem. Z.*, 1916, **76**, 107–176.
41 V. Srinivas and D. Balasubramanian, When does the switch from hydrotropy to micellar behavior occur?, *Langmuir*, 1998, **14**, 6658–6661.
42 T. K. Hogdgon and E. W. Kaler, Hydrotropic solutions, *Curr. Opin. Colloid Interface Sci.*, 2007, **12**, 121–128.
43 J. Eastoe, M. H. Hatzopoulas and P. J. Dowding, Action of hydrotropes and alkyl-hydrotropes, *Soft Matter*, 2011, **7**, 5917–5925.
44 D. Subramanian, J. B. Klauda, J. Leys and M. A. Anisimov, Thermodynamic anomalies and structural fluctuations in aqueous solutions of tertiary butyl alcohol, *Вестник СПбГУ (Herald of St. Petersburg University)*, 2013, **4**, 140–153. Available at: http://arxiv.org/abs/1308.3676.

 This journal is © The Royal Society of Chemistry 2013

Published on 17 June 2013. Downloaded by National Institutes of Standards & Technology on 04/12/2013 20:37:51.

45 J. B. Ott, J. R. Goates and B. A. Waite, (Solid+liquid) phase equilibria and solid-hydrate formation in water + methyl, + ethyl, + isopropyl, and + tertiary butyl alcohols, *J. Chem. Thermodyn.*, 1979, **11**, 739–746.
46 A. Fiore, V. Venkateshwaran and S. Garde, Trimethylamine N-oxide (TMAO) and tert-butyl alcohol (TBA) at hydrophobic interfaces: Insights from molecular dynamics simulations, *Langmuir*, 2013, **29**, 8017–8024.
47 K. Nishikawa and T. Iijima, Structural study of *tert*-butyl alcohol and water mixtures by X-ray diffraction, *J. Phys. Chem.*, 1990, **94**, 6227–6231.
48 H. Tanaka, K. Nakanishi and K. Nishikawa, Clathrate-like structure of water around some nonelectrolytes in dilute solution as revealed by computer simulation and X-ray diffraction studies, *J. Inclusion Phenom.*, 1984, **2**, 119–126.
49 J. Jacob, M. A. Anisimov, J. V. Sengers, A. Oleinikova, H. Weingärtner and A. Kumar, Novel phase-transition behavior near liquid-liquid critical points of aqueous solutions: Formation of a third phase at the interface, *Phys. Chem. Chem. Phys.*, 2001, **3**, 829–831.
50 H. W. Horn, W. C. Swope, J. W. Pitera, J. D. Madura, T. J. Dick, G. L. Hura and T. Head-Gordon, Development of an improved four-site water model for biomolecular simulations: TIP4P-Ew, *J. Chem. Phys.*, 2004, **120**, 9665–9678.
51 K. Vanommeslaeghe, E. Hatcher, C. Acharya, S. Kundu, S. Zhong, J. Shim, E. Darian, O. Guvench, P. Lopes, I. Vorobyov and J. A. D. Mackerell, CHARMM general force field: A force field for drug-like molecules compatible with the CHARMM all-atom additive biological force fields, *J. Comput. Chem.*, 2010, **31**, 671–690.
52 L. Martínez, R. Andrade, E. G. Birgin and J. M. Martínez, PACKMOL: A package for building initial configurations for molecular dynamics simulations, *J. Comput. Chem.*, 2009, **30**, 2157–2164.
53 J. C. Phillips, R. Braun, W. Wang, J. Gumbart, E. Tajkhorshid, E. Villa, C. Chipot, R. D. Skeel, L. Kale and K. Schulten, Scalable molecular dynamics with NAMD, *J. Comput. Chem.*, 2005, **26**, 1781–1802.
54 T. Darden, D. York and L. Pedersen, Particle Mesh Ewald - an NLog(N) Method for Ewald Sums in Large Systems, *J. Chem. Phys.*, 1993, **98**, 10089–10092.
55 S. E. Feller, Y. Zhang, R. W. Pastor and B. R. Brooks, Constant pressure molecular dynamics simulation: The Langevin piston method, *J. Chem. Phys.*, 1995, **103**, 4613–4621.
56 G. J. Martyna, D. J. Tobias and M. L. Klein, Constant pressure molecular dynamics algorithms, *J. Chem. Phys.*, 1994, **101**, 4177–4189.
57 W. Humphrey, A. Dalke and K. Schulten, VMD: Visual molecular dynamics, *J. Mol. Graphics*, 1996, **14**, 33–38.
58 B. J. Berne and R. Pecora, *Dynamic Light Scattering: With Applications to Chemistry, Biology, and Physics*, Wiley, New York, 1976; Dover Publications, Mineola, New York, 2000.
59 B. Chu, *Laser Light Scattering: Basic Principles and Practice*, Academic Press, Boston1991.
60 K. Kasraian and P. P. DeLuca, Thermal analysis of the tertiary butyl alcohol- water system and its implications on freeze-drying, *Pharm. Res.*, 1995, **12**, 484–490.
61 P. K. Kipkemboi and A. J. Easteal, Densities and viscosities of binary aqueous mixtures of nonelectrolytes: *tert*-butyl alcohol and *tert*-butylamine, *Can. J. Chem.*, 1994, **72**, 1937–1945.
62 K. Nakanishi, Partial molal volumes of butyl alcohols and of related compounds in aqueous solution, *Bull. Chem. Soc. Jpn.*, 1960, **33**, 793–797.
63 G. Roux, D. Roberts, G. Perron and J. E. Desnoyers, Microheterogeneity in aqueous organic solutions: Heat capacities, volumes and expansibilities of some alcohols, aminoalcohol and tertiary amines in water, *J. Solution Chem.*, 1980, **9**, 629–647.
64 M. A. Anisimov, V. S. Esipov, V. M. Zaprudskii, N. S. Zaugol'nikova, G. I. Ovodov, T. M. Ovodova and A. L. Seifer, Anomaly in the heat capacity and structural phase transformation of the ordering type in an aqueous solution of *t*-butanol, *J. Struct. Chem.*, 1977, **18**, 663–670.
65 C. De Visser, G. Perron and J. E. Desnoyers, The heat capacities, volumes and expansibilities of *tert*-butyl alcohol–water mixtures from 6 to 65 °C, *Can. J. Chem.*, 1977, **55**, 856–862.
66 Y. Koga, Excess partial molar enthalpies of water in water-*tert*-butanol mixtures, *Can. J. Chem.*, 1988, **66**, 3171–3175.
67 Y. Koga, Differential heats of dilution of *tert*-butanol in water-*tert*-butanol mixtures at 26.90 °C, *Can. J. Chem.*, 1986, **64**, 206–207.
68 Y. Koga, Excess partial molar enthalpies of *tert*-butanol in water-*tert*-butanol mixtures, *Can. J. Chem.*, 1988, **66**, 1187–1193.
69 Y. Koga, W. Y. U. Siu and T. Y. H. Wong, Excess partial molar free energies and entropies in aqueous *tert*-butyl alcohol solutions, *J. Phys. Chem.*, 1990, **94**, 7700–7706.
70 W. S. Knight, *Ph.D Dissertation*, Princeton University, 1962.

Published on 17 June 2013. Downloaded by National Institutes of Standards & Technology on 04/12/2013 20:37:51.

71 M. A. Anisimov, *Critical Phenomena in Liquids and Liquid Crystals*, Gordon & Breach Science Publishers, New York, 1991.
72 K. Tamura, A. Osaki and Y. Koga, Compressibilities of aqueous *tert*-butanol in water-rich region at 25 °C: Partial molar fluctuations and mixing schemes, *Phys. Chem. Chem. Phys.*, 1999, **1**, 121–126.
73 P. Losada-Perez and J. Thoen, KU Leuven, Personal Communication, 2012.
74 E. D. Sloan and C. A. Koh, *Clathrate Hydrates of Natural Gases*, Taylor and Francis, Boca Raton, FL, 2008.
75 G. Gompper and M. Schick, *Self-Assembling Amphiphilic Systems, Volume 16 Phase Transitions and Critical Phenomena*, Academic Press, London, 1994.
76 D. Subramanian and M. A. Anisimov, Mesoscale solubilization in aqueous solutions of hydrotropes, special issue of Fluid Phase Equilibria: *Proceedings of the Conference on Properties and Phase Equilibria for Process and Product Design*, *Fluid Phase Equilib.*, 2013, (in press). Available at: http://arxiv.org/abs/1309.7255.
77 F. H. Stillinger, Structure in aqueous solutions of nonpolar solutes from the standpoint of scales-particle theory, *J. Solution Chem.*, 1973, **2**, 141–158.
78 L. R. Pratt and D. Chandler, Theory of hydrophobic effect, *J. Chem. Phys.*, 1977, **67**, 3683–3704.
79 K. Lum, D. Chandler and J. D. Weeks, Hydrophobicity at small and large length scales, *J. Phys. Chem. B*, 1999, **103**, 4570–4577.
80 A. Häbich, W. Ducker, D. E. Dunstan and X. Zhang, Do stable nanobubbles exist in mixtures of organic solvent and water?, *J. Phys. Chem. B*, 2010, **114**, 6962–6967.

 This journal is © The Royal Society of Chemistry 2013